DTU Library

Cryogenic characterization of titanium nitride thin films

**Vertchenko, Larissa; Leandro, Lorenzo; Shkondin, Evgeniy; Takayama, Osamu; Bondarev, Igor V.;
Akopian, Nika; Lavrinenko, Andrei V.**

Link back to DTU Orbit

Cryogenic characterization of titanium nitride thin films

LARISSA VERTCHENKO,[1,*] LORENZO LEANDRO,[1] EVGENIY SHKONDIN,[1,2] OSAMU TAKAYAMA,[1] IGOR V. BONDAREV,[3] NIKA AKOPIAN,[1] AND ANDREI V. LAVRINENKO[1]

[1]*Department of Photonics Engineering, Technical University of Denmark, Ørsteds Plads 343, DK-2800 Kongens Lyngby, Denmark*
[2]*National Center for Micro- and Nanofabrication (Nanolab), Technical University of Denmark, Ørsteds Plads 347, DK-2800 Kongens Lyngby, Denmark*
[3]*Math and Physics Department, North Carolina Central University, Durham, NC 27707, USA*
[*]lariv@fotonik.dtu.dk

Abstract: It is well known that noble metals are not compatible with silicon fabrication processing due to their low melting point, and that their plasmonic behaviour suffers from the material losses at visible wavelengths. As an alternative, titanium nitride has been highly investigated in order to overcome these challenges. High temperature characterization of TiN films has been performed, showing its CMOS compatibility; however, information on intrinsic losses at lower temperatures is still lacking. Here we experimentally investigate the optical properties of a 100 nm TiN film under low temperatures down to 1.5 K. From the reflection measurements we retrieve the dielectric constant and analyze plasmonic applications possibilities.

1. Introduction

The dielectric response function of a material is related to many optical phenomena and can give insights into more fundamental properties such as free carrier mobility and plasmon resonances. These properties are essential to explore the field of plasmonics [1] which deals with the coupling between the photon radiation and free electrons in metals, giving rise to electromagnetic oscillations on metallic components to result in the strong photon energy confinement on the subwavelength scale [2]. Noble metals such as gold or silver, have exceptional plasmonic properties at visible frequencies, being great materials to manipulate and confine light on the nanometer scale [3]. However, they exhibit high losses at optical frequencies which arise from interactions corresponding to electron-electron, electron-phonon and interband transitions, limiting their plasmonic performances [4]. Another challenge is that they have relatively low melting points — an obstacle that makes them incompatible with semiconductor fabrication processes necessary to develop on-chip CMOS (complementary metal-oxide semiconductor) device applications [5].

Transition metal nitrides have emerged as a new class of materials with the great promise of substituting metals while sharing close optical properties with them [6]. One material that has been under study in recent years is titanium nitride (TiN). Due to its similarity with gold, including the plasmonic response in the visible and near infrared range, it has the advantage of having the high melting point and therefore being chemically stable and so CMOS compatible over a broad temperature range. Various applications for TiN have been pointed out such as biosensing [7], photothermal applications [8], high resistance coatings [9] and metamaterials fabrication [10]. More recently, TiN has been studied as an alternative epsilon-near-zero (ENZ) material in the visible range — material that has the permittivity and refractive index close to zero, leading to interesting effects such as the nonlinearity enhancement [11] and tunneling in waveguides to improve optical transmission properties [12,13].

It has been shown previously that the permittivity of TiN films of variable thickness is greatly dependent on temperature and fabrication methods [14,15], however, only the range above 20 °C was analyzed in the temperature-dependent studies. Moreover, aside from the *dc* conductivity measurements for superconductor applications [16–18], no studies of the dielectric response function and its plasmonic implications at low temperatures were reported so far to the best of our knowledge.

In this work, we describe the fabrication and characterization of a 100 nm film of TiN subjected to low temperatures down to 1.5 K. From the reflection data analysis we were able to retrieve the real and imaginary parts of the dynamical dielectric permittivity function and consequently the refractive index in the visible range. At the ENZ wavelength, around 700 nm, our results show a 4 times decrease in the imaginary part of the permittivity indicating greatly reduced losses. We also evaluate the quality factors for localized surface plasmons (LSPR) and surface plasmon polaritons (SPP) as well as the SPP propagation length (L_{SPP}), in order to elucidate the potential of TiN as a new plasmonic material for the development of on-chip device applications.

2. Experimental realization

Three different samples were fabricated and assembled in a class 100 clean room facility (DTU Nanolab). For the substrates, n-doped Si (100) wafers were selected and cleaned in O_2/N_2 plasma. First, the deposition of a 100 nm TiN layer has been performed by atomic layer deposition technique (Picosun R-200 Advanced Plasma ALD) that allows precise thickness control at sub-nanometer level. The precursors used for TiN deposition were titanium tetrachloride, $TiCl_4$ (from Sigma-Aldrich), and ammonia NH_3. The deposition temperature was chosen to be 500 ^{o}C. The growth rate of TiN (0.025 nm per cycle) was determined by a standard ellipsometry characterization of thicknesses and optical constants (VASE, J.A. Woollam Co.). More information about the fabrication methods can be found at *Shkondin et al* [7]. For the second sample, deposition of 100 nm aluminum thin film has been performed using a conventional electron beam evaporation method (Wordentec QCL 800) at a deposition rate fixed to 5.0 Å/s. Lastly, the third sample constitutes of just the 500 μm double side polished Si wafer. The prepared samples were cleaved in small pieces by an automatic dicing saw (Disco DAD 321) and cleaned by mixture of acetone and isopropanol in a ultrasonic bath, followed by rinsing in a deionized water.

The characterization of the TiN film was conducted by spectroscopic ellipsometry, at room temperature. By employing this technique we were able to evaluate the dielectric function of TiN and retrieve the parameters of the Drude-Lorentz (DL) model [19] of the form

$$\varepsilon(\omega) = \varepsilon_\infty - \frac{\omega_p^2}{\omega^2 + i\Gamma\omega} + \sum_n \frac{S_n\omega_n^2}{\omega_n^2 - \omega^2 - i\gamma_n\omega}. \tag{1}$$

Here, in the Drude term, ε_∞ is the high-frequency dielectric constant, ω_p is the frequency of the plasma oscillations and Γ is its (Drude) damping parameter. In the Lorentz term, the parameters S, ω_n and γ stand for the oscillator strength, transition frequency and (Lorentz) damping, respectively.

In order to reach low temperatures all the samples were placed inside a closed-cycle low-vibration He cryostat. The experimental set up is depicted in Fig. 1. A continuum light source (SuperK from NKT Photonics A/S), with emission wavelength between 350-2400 nm, is directed towards the cryostat and reaches an optical lens, focusing the light spot on one sample each time, under normal incidence. The samples are placed on a moving 3 dimensional piezoelectric translation stages for fine positioning and focusing. The reflected light is redirected towards a mirror and collected by the spectrometer. The reflected signal was analyzed within the range of 600-950 nm.
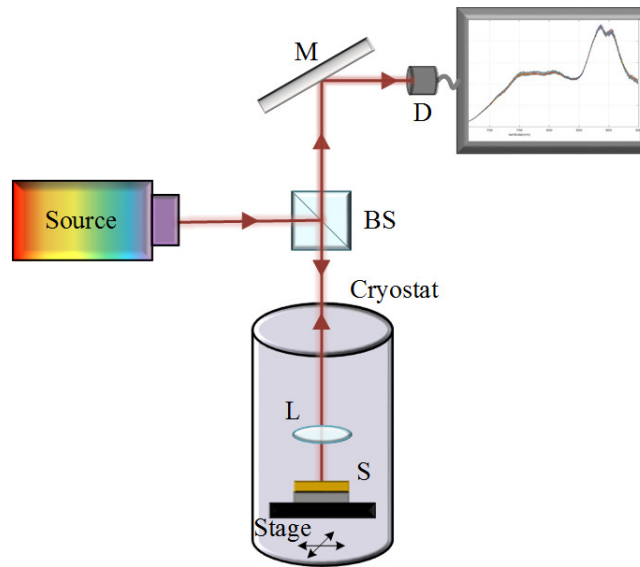
Fig. 1. Experimental setup. Light from the continuum source is directed towards the cryostat through a beam splitter (BS). The light is then focused by an optical lens (L) on one sample (S) each time. Reflected signal is redirected by another mirror (M) to the detector (D) and analyzed. The ice flake symbolizes the low temperature reached inside the cryostat.

We performed reflection measurements of all three samples for 14 different temperatures (200 K, 150 K, 100 K, 75 K, 50 K, 37 K, 25 K, 18 K, 12 K, 6 K, 4.5 K, 3 K and 1.5 K), in addition to the room temperature measurements at 293 K. The reflectance data acquired from the TiN was normalized by the data from the Al mirror and averaged. Afterwards, a fitting procedure was done using the free software RefFit [20], aiming to get the parameters from the DL model [21]. The reference values at room temperature were used and small deviations in the DL terms were applied to have a better fit for each temperature. These reference values at room temperature are necessary, because the system can have good fitting possibilities for different parameters. So the reference imposes a restriction to the choices of the DL terms, making the fitting procedure more reliable. The DL parameters acquired from ellipsometry data at room temperature are presented in Table 1 and Table 2. Since the Drude term is responsible to describe the free electrons, it has been shown that temperature would affect primarily this term [4]. Therefore we have decided to vary mostly the Drude term to reach a better fitting, specially the plasma frequency ω_p and the Drude damping, γ.

Table 1. Parameters of the Drude terms for the permittivity of a 100 nm thick TiN film measured at room temperature

ε_∞	ω_p (THz)	Γ (THz)
4.564	6413.6	488.04

The approach to retrieve the permittivity values of the material is based on the transfer matrix method [22], where each material measured in the cryostat would represent a layer, considering the Al sample as a reference mirror. The model consists of a three-layer system made of TiN, Si and Al, in this order. From the normalized reflectance analysis we obtained the curves for complex permittivity ($\varepsilon = \varepsilon_1 + i\varepsilon_2$) and refractive index ($N = n + i\kappa$), shown in Fig. 2 as functions of the wavelength. For better visualization some of the intermediate values of temperature were omitted.

Table 2. Parameters of the Lorentzian terms for the permittivity of a 100 nm thick TiN film measured at room temperature

n	S_n	ω_n (THz)	γ_n (THz)
1	1.5462	5568.2	2149
2	4.9985	8382	3806.1
3	28.4927	1282.3	1193.4
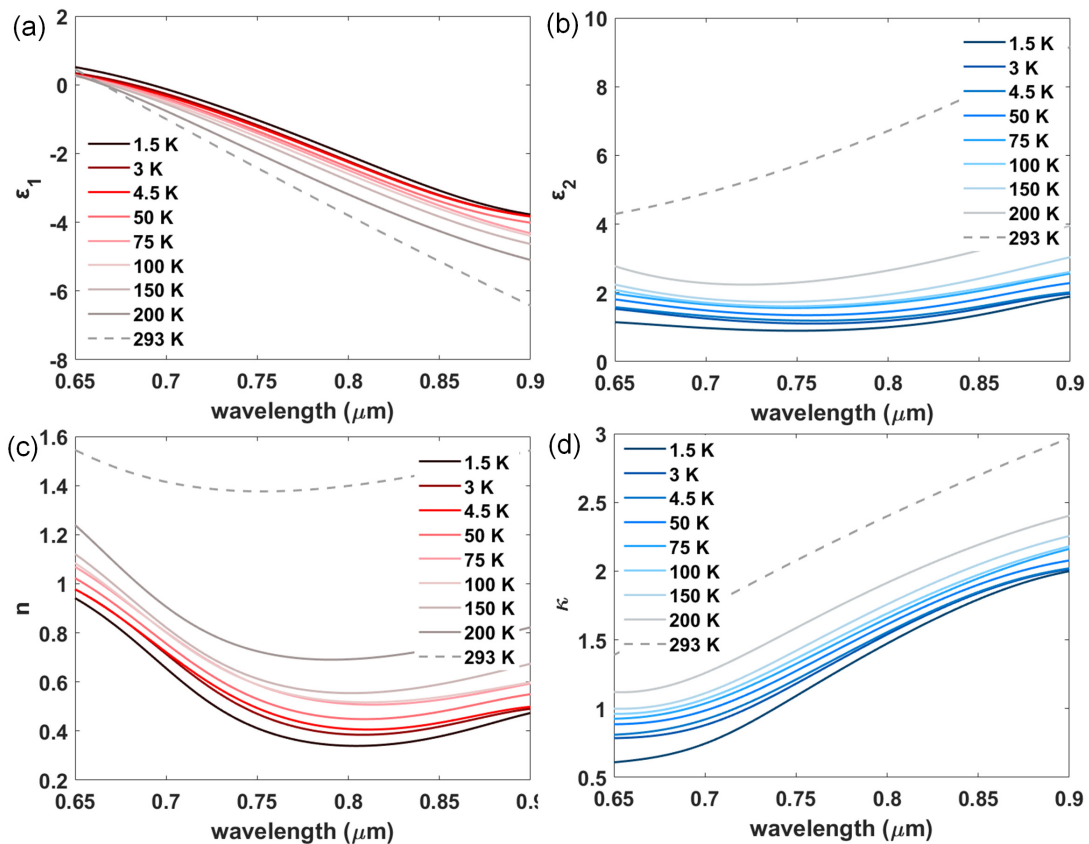
Fig. 2. Real (a,c) and imaginary (b,d) parts of the permittivity ($\varepsilon = \varepsilon_1 + i\varepsilon_2$) and refractive index ($N = n + i\kappa$), respectively, for a 100 nm TiN film for different temperatures, as a function of the wavelength. The color coding is depicted in the legends.

3.　Results and discussion

From the experimental results and the reconstruction of the dielectric response function and refractive index, it is possible to observe a decrease in the imaginary part ε_2 of the permittivity as the temperature decreases. Such a behavior was also verified by Jayanti el at. [23] with temperature dependent measurements performed on Ag films. It was explained in terms of the reduction of the electron-phonon scattering rate with decreasing temperature. In our case for temperature 1.5 K at the ENZ wavelength where ε_1 is close to zero, Fig. 3(a) shows the decrease of ε_2 by a factor of 4 (from 4 down to 1) as compared to the room temperature value, indicating a significant loss reduction at low temperature.
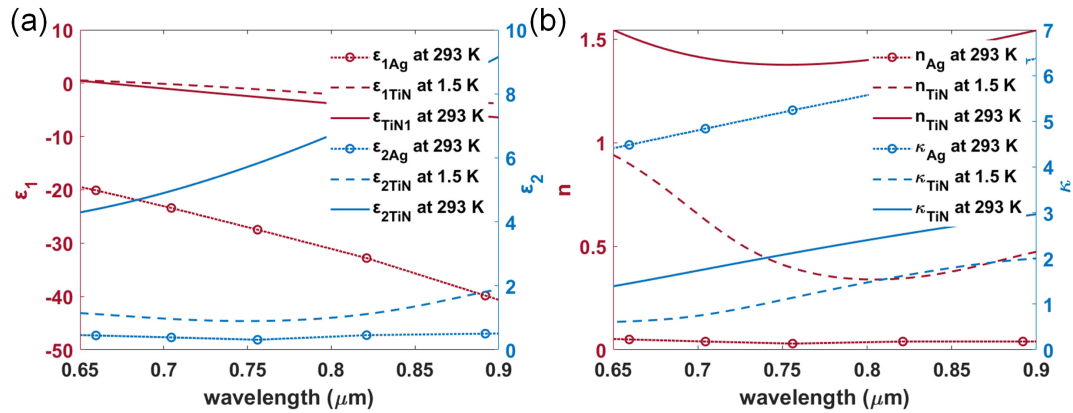

Fig. 3. (a) Comparison between the real (ε_1) and imaginary (ε_2) parts of the dielectric function for Ag at 293 K, TiN at 1.5 K and TiN at 293 K, as a function of the wavelength. (b) Real (n) and imaginary (κ) parts of the refractive index at the same conditions.

Whereas the complex permittivity is related to scattering and absorption, the refractive index can be associated with the propagation properties such as transmission and reflection. By comparing the results of the refractive index measurements for TiN to those for Ag as depicted in Fig. 3(b), we observe a great improvement in the TiN attenuation factor κ, which is responsible for the exponential decrease of the amplitude of propagating electromagnetic waves, to exhibit much better optical transmission properties for TiN.

Figure 4 shows the imaginary part ε_2 of the complex permittivity at the ENZ wavelength ($\varepsilon_1 = 0$) and the plasma oscillations wavelength λ_p as functions of the cryostat temperature. Above 100 K bigger error bars are expected due to noise and more difficulties in temperature stabilization control. From the plot one can see a tiny gradual decrease in the plasma wavelength as temperature goes up all the way from $T \sim 4$ K. This can be ascribed to the counteracting effects of the electron density and effective mass reduction as discussed previously in Ref. [15]. One can therefore conclude that the ENZ wavelength of our TiN samples, which is very close to λ_p for not too short wavelengths according Eq. (1), is hardly affected by the temperature change except for $T \lesssim 4$ K where ε_2 drops down abruptly because of λ_p going rapidly up (with ω_p quickly decreasing accordingly). We also see that ε_2 at the ENZ wavelength follows a linear tendency down to approximately 4 K. The linear regression fitting procedure using for $\varepsilon_2(T)$ the model function $f(T) = AT + B$ (excluding the lowest temperature point) gives $A = 0.0056$ and $B = 1.37$ with the fit goodness $R^2 = 0.98$ shown by the red line in the figure.

To understand the peculiar temperature dependence below 4 K in Fig. 4 we use the confinement induced nonlocal dielectric response model developed recently for plasmonic films of finite variable thickness [24,25]. The model is based on the fact that for visible to near-infrared frequencies (well below the interband transition frequencies) the thin film response of Eq. (1)
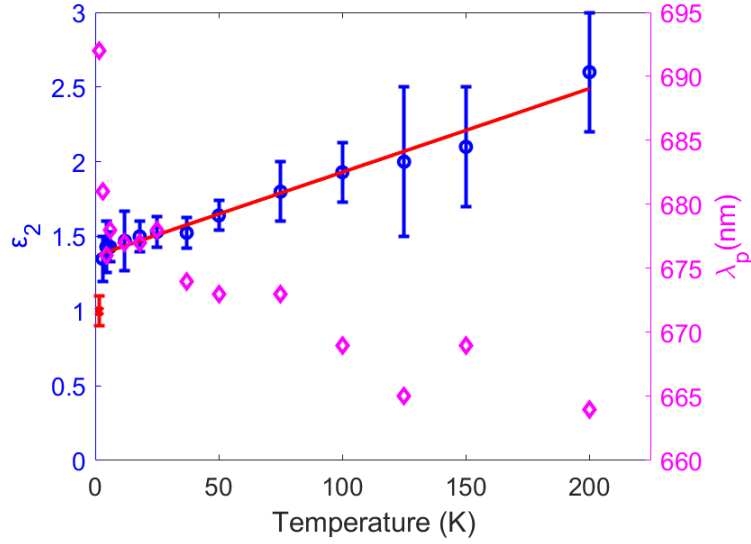
Fig. 4. Plots of the imaginary part of the complex permittivity at the ENZ point (blue circles) and the plasma wavelength (diamonds) as functions of the sample temperature. The red line represents the linear fit performed on the imaginary part of the permittivity with the lowest temperature data point (red square at 1.5 K) being excluded.

can be represented as a nonlocal Drude dielectric response function $\varepsilon(k, \omega)$ defined as

$$\frac{\varepsilon(k, \omega)}{\varepsilon_b} = 1 - \frac{\omega_p^2(k)}{\omega^2 + i\Gamma\omega} = 1 - \frac{\omega_p^2(k)}{\omega^2 + \Gamma^2}\left(1 - i\frac{\Gamma}{\omega}\right). \tag{2}$$

Here, ε_b is the real constant to account for the effect of the background dielectric screening in the film material [26] (contributed by the Lorentz term and ε_∞),

$$\omega_p(k) = \frac{\omega_p^{3D}}{\sqrt{1 + (\varepsilon_{sb} + \varepsilon_{sp})/\varepsilon_b kd}}, \tag{3}$$

is the in-plane plasma oscillation frequency of the electron gas with the 2D plasmon momentum $k (= |\mathbf{k}|)$ in the film of thickness d sandwiched between the substrate and superstrate with the dielectric constants ε_{sb} and ε_{sp}, respectively, and $\omega_p^{3D} = \sqrt{4\pi e^2 N_{3D}/\varepsilon_b m^*}$ is the plasma frequency of the bulk (3D) plasmonic material with N_{3D} and m^* being the volumetric electron density and electron effective mass, respectively. The plasma frequency in Eq. (3) is spatially dispersive, to result in the nonlocal dielectric response in Eq. (2), because of the pair Coulomb interaction potential modification due to the vertical confinement of the charges in the finite-thickness plasmonic films [24].

The standard procedure of the thermal averaging of Eq. (3) reads

$$\overline{\omega}_p(T) = \frac{\int_0^{k_c} dk k\, \omega_p(k)/\{\exp[\hbar\omega_p(k)/k_B T] - 1\}}{\int_0^{k_c} dk k/\{\exp[\hbar\omega_p(k)/k_B T] - 1\}}, \tag{4}$$

where the numerator sums up all boson plasma frequency modes with different k and the denominator provides the total number of such modes available in the 2D k-space (bounded

above by k_c the plasmon cutoff parameter). Substituting Eq. (3) in Eq. (4) one obtains

$$\frac{\overline{\omega}_p(T)}{\omega_p^{3D}} = \frac{\int_0^1 dt\, t\sqrt{\frac{t}{t+1/a}}/[\exp\left(\alpha\sqrt{\frac{t}{t+1/a}}\right)-1]}{\int_0^1 dt\, t/[\exp\left(\alpha\sqrt{\frac{t}{t+1/a}}\right)-1]}. \tag{5}$$

Here, $\alpha = \hbar\omega_p^{3D}/k_B T$ and $a = \varepsilon_b k_c d/(\varepsilon_{sb} + \varepsilon_{sp})$ control the plasma frequency T-dependence through the film thickness parameter d at all other things being equal. Both for $a \to \infty$ (very thick films) and for $a \to 0$ (ultrathin films) Eq. (5) is seen to be essentially T-independent. In the latter case, the plasma frequency goes down as $\sqrt{d}$ — the effect previously discussed theoretically [24,25] and observed experimentally for ultrathin TiN films at ambient temperature [27,28]. Away from these two extremes there is a T-dependence stemming from $\alpha\sqrt{t/(t + 1/a)}$, with the denominator being always greater than the numerator as $\sqrt{t/(t + 1/a)}<1$ to result in a sudden drop of $\overline{\omega}_p$ with lowering the temperature. Figure 5(a) shows the general behavior of the plasma frequency as a function of (dimensionless) temperature and film thickness as given by Eq. (5).
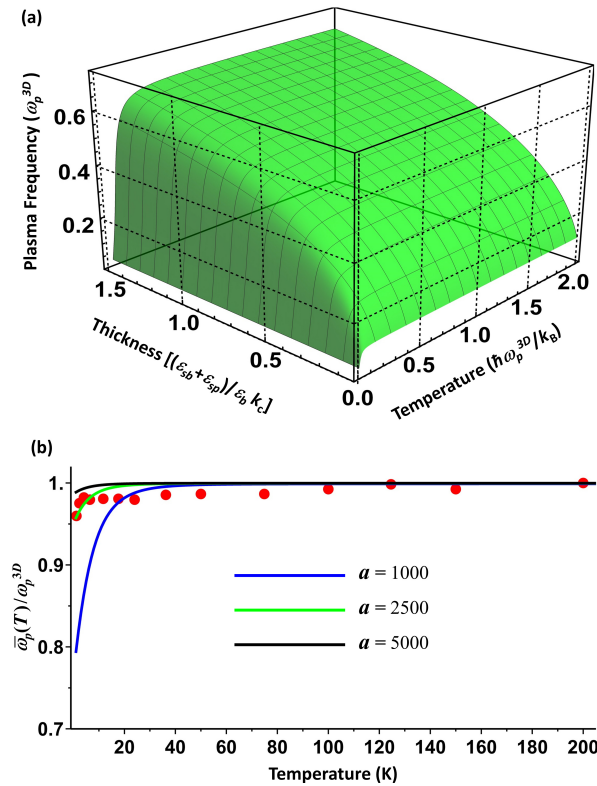

Fig. 5. (a) Plasma frequency general behavior as a function of dimensionless temperature and film thickness as computed from Eq. (5). (b) Analysis of the plasma frequency temperature dependence using the confinement induced nonlocal dielectric response model of the finite-thickness plasmonic film [24]. See text for details.

The experimental data in Fig. 4 can now be understood in terms of Eqs. (2) and (5). The results of our plasma frequency analysis are presented in Fig. 5(b). The dots there show the ratio $\overline{\omega}_p(T)/\omega_p^{3D}$ obtained from the data set in Fig. 4(a) with ω_p^{3D} approximated by $2\pi c/\lambda_p(200 \text{ K}) = 1.867$ eV. The lines are computed from Eq. (5) with $a = 1000$, 2500 and 5000. The green line with $a = \varepsilon_b k_c d/(\varepsilon_{sb} + \varepsilon_{sp}) = 2500$ is seen to follow the data points quite well at all T, reproducing also

the drop at $T < 4$ K. For our films of $d = 100$ nm we then have $k_c \approx 2.5(\varepsilon_{sb} + \varepsilon_{sp})/\varepsilon_b$ Å^{-1}. Using $k_c = 0.64$ Å^{-1} reported recently from the comparison of the Drude model with the first-principle calculations of the low-energy plasmon excitation mode in bulk TiN [29], one now obtains $\varepsilon_b/(\varepsilon_{sb} + \varepsilon_{sp}) \approx 3.9$ to result in $\varepsilon_b \approx 7.8$ and $\varepsilon_b \approx 50$ for the 100 nm thick TiN film free-standing in air and for that deposited on Si substrate ($\varepsilon_{sb} = 11.7$), respectively. Different ε_b values obtained reflect the differences in the Coulomb screening for the finite-thickness films immersed in different surroundings [24]. Note that for ultrathin disks of gold $\varepsilon_b = 9.5$ was earlier reported within the framework of a similar Drude model with no confinement induced nonlocality included though [26].

The dielectric function in Eq. (2) allows one to understand the temperature dependence of ε_2 in Fig. 4(b) as well. From Eq. (2) one has $\varepsilon_2 = \mathrm{Im}\,\varepsilon \sim \omega_p^2 \Gamma$ with ω_p being independent of T all the way down to 4 K (neglecting a small effect above-mentioned of the counteracting contributions of the electron density and electron effective mass). Therefore, the linear temperature dependence of ε_2 can only be coming from the Drude damping parameter Γ which is nothing but the inelastic electron scattering rate. For temperatures below 293 K this is known to be mainly contributed by the electron-acoustic-phonon scattering (optical phonons typically have a higher excitation energy threshold [30]) with the scattering rate proportional to $k_B T$ stemming from the long-wavelength acoustic phonon occupation number [31]. Needless to say that the sudden drop of ε_2 below 4 K comes from the drop of $\overline{\omega}_p(T)$ as discussed above. Another tempting, seemingly plausible explanation could be using the known fact of the superconducting phase transition in thin TiN films at $T < 1$ K [17,18] as a factor to drastically affect the low-T electron plasma oscillation frequency. However, the superconducting coherence length of Cooper pairs does not typically exceed a few nanometers, which is a too tiny scale to be able to affect the long-wavelength plasmon dispersion and the plasmon coherence length on the order of a micrometer (let alone the fact of T_c being much less than 4 K at which we start seeing the effect here).

4. Plasmonics

In this section we analyze the plasmonic properties of the measured TiN film at low temperatures. The performance of plasmonic materials depends both on the real part of their complex permittivity function which determines the local field distribution, and on the imaginary part which quantifies the energy losses [4]. The overall performance of the plasmonic film can be characterized by the quality factor Q of the coupled light-matter excitations such as localized surface plasmon resonances (*LSPR*) and surface plasmons polaritons (SPPs) [32].

LSPRs are the static excitations of the conduction electrons coupled to the external electromagnetic field. They result in the local electromagnetic field enhancement. The Q factor for the *LSPR* is described by the ratio of the enhanced local field to the incident field, and depends on the material composition and the geometrical shape of the metallic structure. For a sphere of not too small diameter, for example, the Q_{LSPR} can be represented by the ratio $-\varepsilon_1(\omega)/\varepsilon_2(\omega)$ under the assumption of being mostly contributed by the material composition [4]. For TiN material we then obtain the Q_{LSPR} wavelength and temperature dependence as shown in Fig. 6, where we can see a big improvement as temperature goes down when compared to the room temperature, however we still notice its inferiority to noble metals such as Ag.

Another fundamental excitation in plasmonics is the SPP — the transverse wave formed by the collective electron oscillations coupled to the electromagnetic wave propagating along the metal-dielectric interface. The SPP dispersion relation is given by

$$\beta = \frac{\omega}{c}\sqrt{\frac{\varepsilon\varepsilon_D}{\varepsilon + \varepsilon_D}}, \tag{6}$$

where β is the SPP momentum, c is the speed of light, ε is the complex dynamical dielectric permittivity of the metal and ε_D is the permittivity constant of the dielectric material which we
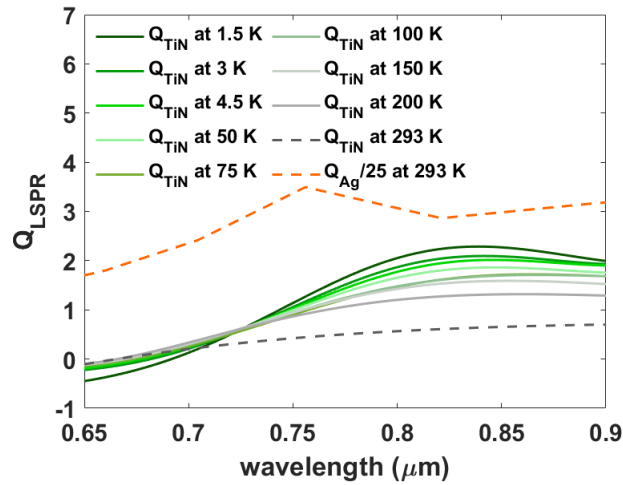
Fig. 6. Quality factor of localized surface plasmons Q_{LSPR} for a TiN sphere of not too small diameter as a function of wavelength and temperature (encoded by colors). The Q_{LSPR} of Ag was divided by 25 in order to maintain the visibility of the other curves.

here assume to be air ($\varepsilon_D = 1$) for simplicity. The propagation of SPPs is controlled by the energy attenuation length defined as $L_{SPP} = (2Im\beta)^{-1}$. The SPP can only be excited provided that the condition $|\varepsilon(\omega)| \geq 1$ is fulfilled. For that reason, we calculate the Q_{SPP} for TiN by analogy with Q_{LSPR} for wavelengths above 750 nm. The plots of Q_{SPP} and L_{SPP} are shown in Fig. 7.
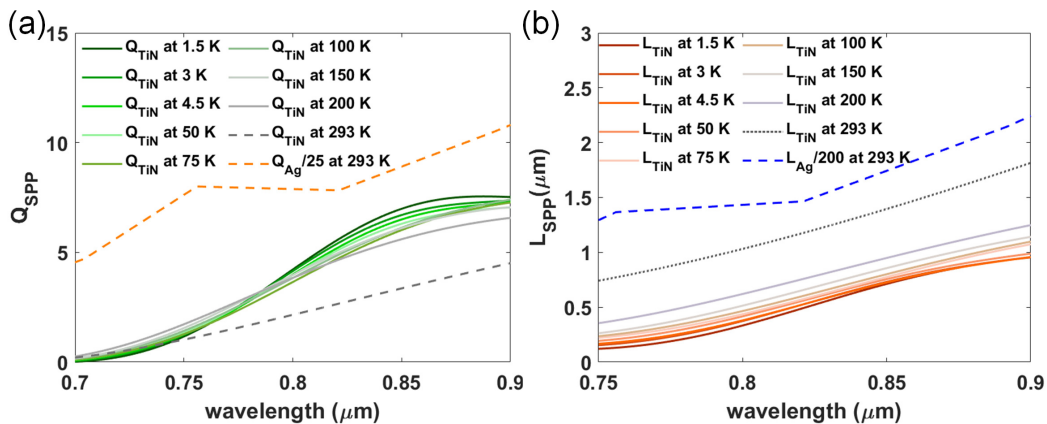

Fig. 7. (a) Q_{SPP} and (b) L_{SPP} for TiN as functions of wavelength at different temperatures. The Q_{SPP} and L_{SPP} of Ag were divided by 25 and 200, respectively, in order to keep the visibility of the other curves.

5. Conclusion

We have experimentally retrieved the complex valued dynamical dielectric permittivity function of a 100 nm TiN film for a broad range of wavelengths and low temperatures down to 1.5 K. Our study shows the 4 times decrease in the imaginary part of the dielectric function around the ENZ wavelength at low temperatures, indicating greatly reduced losses. This results in much better electromagnetic propagation properties for TiN at low temperatures as compared to room

temperature, placing it next to noble metals such as Au and Ag. From the measured temperature dependence of the permittivity imaginary part at the ENZ wavelength we were able to identify and explain theoretically a highly nonlinear regime of the loss reduction below 4 K. We have also performed the analysis of the basic plasmonic properties such as the LSPR and SPP quality factors for the TiN material at different temperatures.

Funding

References

1. S. A. Maier and H. A. Atwater, "Plasmonics: Localization and guiding of electromagnetic energy in metal/dielectric structures," J. Appl. Phys. **98**(1), 011101 (2005).
2. S. Lal, S. Link, and N. J. Halas, "Nano-optics from sensing to waveguiding," Nat. Photonics **1**(11), 641–648 (2007).
3. A. Boltasseva and H. A. Atwater, "Low-loss plasmonic metamaterials," Science **331**(6015), 290–291 (2011).
4. P. R. West, S. Ishii, G. V. Naik, N. K. Emani, V. M. Shalaev, and A. Boltasseva, "Searching for better plasmonic materials," Laser Photon. Rev. **4**(6), 795–808 (2010).
5. A. Boltasseva and V. M. Shalaev, "All that glitters need not be gold," Science **347**(6228), 1308–1310 (2015).
6. G. V. Naik, J. L. Schroeder, X. Ni, A. V. Kildishev, T. D. Sands, and A. Boltasseva, "Titanium nitride as a plasmonic material for visible and near-infrared wavelengths," Opt. Mater. Express **2**(4), 478–489 (2012).
7. E. Shkondin, T. Repän, O. Takayama, and A. V. Lavrinenko, "High aspect ratio titanium nitride trench structures as plasmonic biosensor," Opt. Mater. Express **7**(11), 4171–4182 (2017).
8. S. Ishii, R. Kamakura, H. Sakamoto, T. D. Dao, S. L. Shinde, T. Nagao, and K. Tanaka, "Demonstration of temperature-plateau superheated liquid by photothermal conversion of plasmonic titanium nitride nanostructures," Nanoscale **10**(39), 18451–18456 (2018).
9. H. E. Rebenne and D. G. Bhat, "Review of CVD TiN coatings for wear-resistant applications: deposition processes, properties and performance," Surf. Coat. Technol. **63**(1-2), 1–13 (1994).
10. A. Boltasseva, "Empowering plasmonics and metamaterials technology with new material platforms," MRS Bull. **39**(05), 461–468 (2014).
11. E. G. Carnemolla, L. Caspani, C. DeVault, M. Clerici, S. Vezzoli, V. Bruno, and M. Ferrera, "Degenerate optical nonlinear enhancement in epsilon-near-zero transparent conducting oxides," Opt. Mater. Express **8**(11), 3392–3400 (2018).
12. N. Engheta, "Pursuing near-zero reponse," Science **340**(6130), 286–287 (2013).
13. M. Silveirinha and N. Engheta, "Tunneling of electromagnetic energy through subwavelength channels and bends using epsilon-near-zero materials," Phys. Rev. Lett. **97**(15), 157403 (2006).
14. J. A. Briggs, G. A. Naik, Y. Zhao, T. A. Petach, K. Sahasrabuddhe, D. Goldhaber-Gordon, and J. A. Dionne, "Temperature-dependent optical properties of titanium nitride," Appl. Phys. Lett. **110**(10), 101901 (2017).
15. H. Reddy, U. Guler, Z. Kudyshev, A. V. Kildishev, V. M. Shalaev, and A. Boltasseva, "Temperature-dependent optical properties of plasmonic titanium nitride thin films," ACS Photonics **4**(6), 1413–1420 (2017).
16. F. Pfuner, L. Degiorgi, T. I. Baturina, V. M. Vinokur, and M. R. Baklanov, "Optical properties of TiN thin films close to the superconductor-insulator transition," New J. Phys. **11**(11), 113017 (2009).
17. T. I. Baturina, S. V. Postolova, A. Y. Mironov, A. Glatz, M. R. Baklanov, and V. M. Vinokur, "Superconducting phase transitions in ultrathin TiN films," Europhys. Lett. **97**(1), 17012 (2012).
18. A. Shearrow, G. Koolstra, S. J. Whiteley, N. Earnest, P. S. Barry, F. J. Heremans, and D. I. Schuster, "Atomic layer deposition of titanium nitride for quantum circuits," Appl. Phys. Lett. **113**(21), 212601 (2018).
19. P. Patsalas, N. Kalfagiannis, and S. Kassavetis, "Optical properties and plasmonic performance of titanium nitride," Materials **8**(6), 3128–3154 (2015).
20. A. Kuzmenko, RefFIT, https://reffit.ch/products/, (2016).
21. M. A. Panah, O. Takayama, S. V. Morozov, K. E. Kudryavtsev, E. S. Semenova, and A. V. Lavrinenko, "Highly doped InP as a low loss plasmonic material for mid-IR region," Opt. Express **24**(25), 29077–29088 (2016).
22. C. J. Gabriel and A. Nedoluha, "Transmittance and reflectance of systems of thin and thick layers," Optica Acta: Intl. J. Optics **18**(6), 415–423 (1971).
23. S. V. Jayanti, J. H. Park, A. Dejneka, D. Chvostova, K. M. McPeak, X. Chen, and D. J. Norris, "Low-temperature enhancement of plasmonic performance in silver films," Opt. Mater. Express **5**(5), 1147–1155 (2015).
24. I. V. Bondarev and V. M. Shalaev, "Universal features of the optical properties of ultrathin plasmonic films," Opt. Mater. Express **7**(10), 3731–3740 (2017).
25. I. V. Bondarev, H. Mousavi, and V. M. Shalaev, "Optical response of finite-thickness ultrathin plasmonic films," MRS Commun. **8**(03), 1092–1097 (2018).
26. A. Manjavacas and F. J. Garcia de Abajo, "Tunable plasmons in atomically thin gold nanodisks," Nat. Commun. **5**(1), 3548 (2014).

27. D. Shah, A. Catellani, H. Reddy, N. Kinsey, V. Shalaev, A. Boltasseva, and A. Calzolari, "Controlling the plasmonic properties of ultrathin TiN films at the atomic level," ACS Photonics **5**(7), 2816–2824 (2018).
28. D. Shah, H. Reddy, N. Kinsey, V. M. Shalaev, and A. Boltasseva, "Optical properties of plasmonic ultrathin TiN films," Adv. Opt. Mater. **5**(13), 1700065 (2017).
29. A. Catellani and A. Calzolari, "Plasmonic Properties of Refractory Titanium Nitride," Phys. Rev. B **95**(11), 115145 (2017).
30. I. V. Bondarev, "Delocalized positronium in alkali-halide crystals: analysis of possible lattice-scattering processes," Phys. Lett. A **291**(1), 39–45 (2001).
31. B. K. Ridley, *Quantum Processes in Semiconductors*, 5th edn Oxford, (2013).
32. S. A. Maier, *Plasmonics: Fundamentals and Applications*. Springer Science and Business Media, (2007).